

Cortical Feedback Decorrelates Olfactory Bulb Output in Awake Mice

Highlights

- Piriform feedback to olfactory bulb is sparse, odor specific, and locally diverse
- Distinct feedback axon types enhance or suppress their baseline activity to odors
- Feedback responses are layer selective and can outlast odor stimulation by seconds
- Piriform cortex decorrelates mitral but not tufted cells' odor responses

Authors

Gonzalo H. Otazu, Honggoo Chae,
Martin B. Davis, Dinu F. Albeanu

Correspondence

albeanu@cshl.edu

In Brief

Otazu, Chae et al. describe sparse and odor-specific piriform cortex feedback to olfactory bulb. They find that distinct feedback axonal types are either enhanced or suppressed by odors. Cortical inactivation differentially decorrelates mitral, but not tufted cells odor representations.



Cortical Feedback Decorrelates Olfactory Bulb Output in Awake Mice

Gonzalo H. Otazu,^{1,3} Honggoo Chae,^{1,3} Martin B. Davis,¹ and Dinu F. Albeanu^{1,2,*}

¹Cold Spring Harbor Laboratory, Cold Spring Harbor, NY 11724, USA

²Watson School of Biological Sciences, Cold Spring Harbor, NY 11724, USA

³Co-first author

*Correspondence: albeanu@cshl.edu

<http://dx.doi.org/10.1016/j.neuron.2015.05.023>

SUMMARY

The olfactory bulb receives rich glutamatergic projections from the piriform cortex. However, the dynamics and importance of these feedback signals remain unknown. Here, we use multiphoton calcium imaging to monitor cortical feedback in the olfactory bulb of awake mice and further probe its impact on the bulb output. Responses of feedback boutons were sparse, odor specific, and often outlasted stimuli by several seconds. Odor presentation either enhanced or suppressed the activity of boutons. However, any given bouton responded with stereotypic polarity across multiple odors, preferring either enhancement or suppression. Feedback representations were locally diverse and differed in dynamics across bulb layers. Inactivation of piriform cortex increased odor responsiveness and pairwise similarity of mitral cells but had little impact on tufted cells. We propose that cortical feedback differentially impacts these two output channels of the bulb by specifically decorrelating mitral cell responses to enable odor separation.

INTRODUCTION

Early sensory areas receive massive top-down projections from the cortex, suggesting that this feedback plays a crucial function (Otazu and Leibold, 2011; Rao and Ballard, 1999). Visual, auditory, and somatosensory experiments have proposed several roles for cortical feedback, including sharpening of sensory representations, or relaying information pertaining to expectation, reward, attention, learning, and action (Gilbert and Li, 2013; Glickfeld et al., 2013; Harris and Mrsic-Flogel, 2013; Petreanu et al., 2012). The olfactory bulb (OB), like other early sensory areas, receives abundant feedback projections from cortical areas involved in odor identification, localization, and olfactory memory (Boyd et al., 2012; Markopoulos et al., 2012; Oswald and Urban, 2012; Shepherd, 1972). Although cortical feedback axons outnumber olfactory sensory inputs, their function in shaping the OB output remains unclear to date.

The OB receives glutamatergic feedback mainly from anterior olfactory nucleus (AON), piriform, and entorhinal cortex (Oswald and Urban, 2012; Rothermel and Wachowiak, 2014; Shepherd, 1972; Shipley and Adamek, 1984). The bulb also integrates GABAergic (Nunez-Parra et al., 2013), neuromodulatory (Devore and Linster, 2012; Petzold et al., 2009; Ranade and Mainen, 2009; Wachowiak et al., 2009; Wilson et al., 2004), and hormonal (Tobin et al., 2010) inputs that have been proposed to contextually regulate OB activity during learning and odor discrimination. In this study, we focus on understanding the dynamics and roles of feedback signals from the primary olfactory cortex (piriform) to the bulb.

Previous work has suggested that in complex sensory environments, the piriform cortex reconstructs olfactory objects from degraded noisy stimuli or segments relevant targets from irrelevant, variable backgrounds (Gottfried, 2010; Vickers, 2000; Wilson and Sullivan, 2011). Within this framework, the piriform cortex may act as a pattern-recognition device (Babadi and Sompolinsky, 2014; Barak et al., 2013; Caron et al., 2013; Haberly, 2001; Haberly and Bower, 1989; Linster and Hasselmo, 2001) that compares incoming sensory inputs with representations of previously experienced odors, integrates contextual information, and sends predictive signals to the sensory periphery through massive bulbar feedback projections. Indeed, anatomical tracing studies show that individual anterior piriform cortex (APC) feedback axons follow long, tortuous trajectories across the OB and form clusters of synapses that can lie far apart from each other (Matsutani, 2010).

The output neurons of the OB, the mitral/tufted (MT) cells, project most abundantly in a distributed manner to the piriform cortex and to several other areas including the AON, olfactory tubercle, entorhinal cortex, and amygdala (Ghosh et al., 2011; Miyamichi et al., 2011; Nagayama et al., 2010; Shepherd, 1972; Sosulski et al., 2011). In turn, the primary recipients of these feedback projections are the granule cells (GCs) (Balu et al., 2007; Boyd et al., 2012; Margrie et al., 2001; Urban and Sakmann, 2002; Wilson and Mainen, 2006). Piriform cortex feedback axons also establish sparser synapses with deep short axon cells, which inhibit the GCs, and with interneurons in the glomerular layer (periglomerular and superficial short axon cells) (Boyd et al., 2012; Matsutani, 2010). Thus, cortical feedback axons act indirectly on MT cells via OB inhibitory interneurons.

Studies in anesthetized rodents have proposed that cortical feedback provides non-specific, global inhibitory gain control to prevent runaway saturation of MT cell firing. Electrical

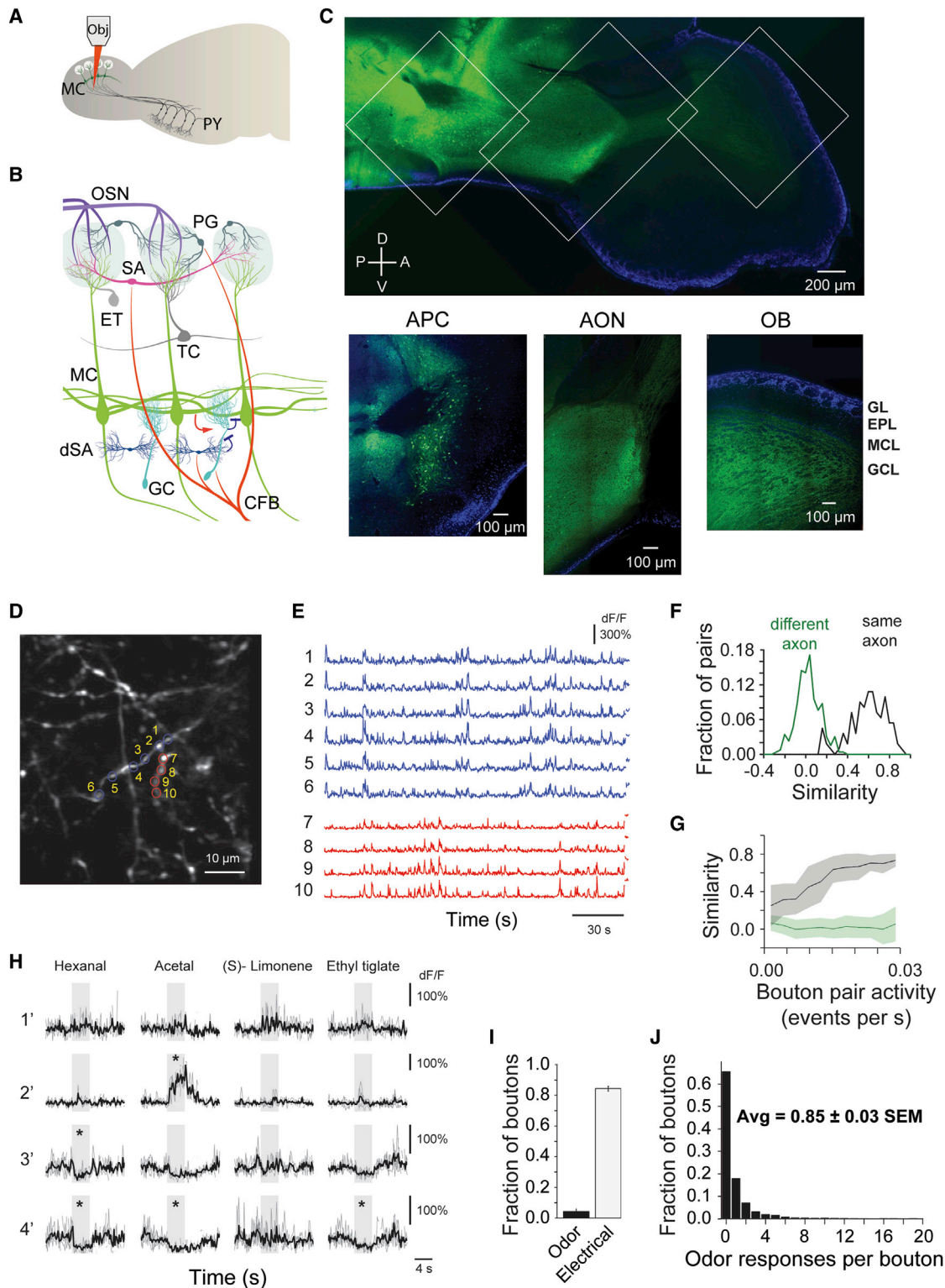


Figure 1. Monitoring Corticalbulbar Boutons in Awake Head-Fixed Mice via Multiphoton Imaging of GCaMP5 Signals

(A) Schematics of experimental setup: optical monitoring of cortical-bulbar feedback bouton responses via multiphoton imaging of GCaMP5 signals; Obj, 2p microscope objective; MC, mitral cells; Py, pyramidal neurons in the anterior piriform cortex (APC).

(B) Olfactory bulb (OB) circuit and neuronal types; OSN, olfactory sensory neurons; PG, periglomerular cells; SA, superficial short axon cells; ET, external tufted cells; TC, tufted cells; MC, mitral cells; dSA, deep short axon cells; GC, granule cells; CFB, cortical feedback fibers.

(legend continued on next page)

(Nakashima et al., 1978) or optogenetic (Boyd et al., 2012) activation of the feedback projections has been shown to suppress odor-evoked MT cell responses. These results cannot easily be extrapolated to awake animals, since cortical feedback could be modulated by context and expectation and may follow substantially different dynamics (Gilbert and Li, 2013; Harris and Mrsic-Flogel, 2013). In addition, piriform cortex inactivation in awake rabbits has been shown to synchronize MT cells, while decreasing their firing rate, which contradicts the findings from anesthetized mice (Gray and Skinner, 1988).

To date, it remains unknown whether the impact of piriform cortex feedback varies across the two main output populations of the bulb, the mitral and tufted cells, which reside in different anatomical layers. Recent work indicates that mitral and tufted cells differ in response properties (Burton and Urban, 2014; Fukunaga et al., 2012; Igarashi et al., 2012; Manabe and Mori, 2013; Nagayama et al., 2004) and project differentially to downstream brain areas, with stronger tufted cell innervation of the AON compared to the piriform cortex (Igarashi et al., 2012).

Here, we characterized the response properties of cortical bulbar boutons in awake head-fixed mice across bulb layers as a function of odor identity and concentration via multiphoton imaging of GCaMP5 signals (Figures 1A and 1B). Furthermore, we employed pharmacological suppression of neuronal activity in the APC in conjunction with optical monitoring of both mitral and tufted cells activity to determine the contribution of top-down cortical inputs in shaping sensory processing in the bulb.

RESULTS

We expressed the genetically encoded calcium indicator GCaMP5 (Tian et al., 2009) in the APC under the control of the *EF1 α* promoter using adeno-associated viruses (AAV2.9). To ensure homogeneous labeling of the APC, we performed multiple bilateral injections (see Experimental Procedures). Confocal imaging of DAPI signals and GCaMP5 fluorescence in sagittal slices showed robust labeling of cell bodies in the APC and abundant neuropil in the OB and AON (Figure 1C; Figure S1A). No fluorescent cell bodies could be detected in the OB. In the bulb, the density of GCaMP5-labeled boutons was highest in the GCL, but axonal projections were also present in the glomerular and external plexiform layers (Figures 1B and 1C; Figures

S1C and S1D). Consistent with previous reports of lack of GABAergic feedback from the piriform cortex (Boyd et al., 2012), we did not find expression of GCaMP5 in feedback axons upon injection of *EF1 α -FLEX-GCaMP5* AAV2.9 in the APC of *GAD65-Cre* mice (Figure S1B; Taniguchi et al., 2011).

Corticalbulbar Feedback Projections Are Spontaneously Active and Show Sparse and Odor-Specific Responses

To date, little is known about corticobulbar feedback activity in awake or anesthetized animals. One recent study investigated the dynamics of AON-to-bulb feedback boutons in the glomerular layer (Rothermel and Wachowiak, 2014). As a first step toward understanding the functional roles of corticobulbar feedback projections, we characterized their spontaneous dynamics and responses to a diverse panel of 20 odors (Odor Set A, Table S1), using multiphoton imaging of GCaMP5 signals in awake head-fixed mice (Figures 1A and 1D; Figures S1E–S1G, see Experimental Procedures). We started by monitoring feedback axons innervating the deep OB layers (200–350 μ m from surface), since these represent the highest number of corticobulbar projections (Figures S1C and S1D).

Approximately 23% of the imaged boutons (5,221 boutons, 18 fields of view, 4 mice) showed locally diverse and brief (<1 s) spontaneous activity bouts (Figures 1D and 1E, Figures S1H, S2A, and S2B, Movie S1, see Experimental Procedures). Boutons anatomically assigned to the same axonal branch (see Experimental Procedures) showed significantly higher correlations than boutons belonging to different branches in a given field of view (FOV) (average = 0.60 ± 0.02 versus average = 0.03 ± 0.01 , values indicate mean \pm SEM unless specified otherwise, 52 axonal segments, 337 pairs of boutons from the same axon, 648 pairs of boutons from different axons, $p < 0.001$, Wilcoxon rank-sum test, Figures 1F and 1G; Figure S1H). As expected, correlations in spontaneous activity of boutons on the same axon (Petreanu et al., 2012) were higher for bouton pairs that had high levels of spontaneous activity (Figure 1G).

To determine whether an odor response was significant, we compared the average fluorescence change during odor presentation with a bootstrap distribution of average fluorescence calculated over baseline periods of equal length preceding odor presentation (threshold = 99.9th percentile of bootstrap

(C) Top: composite GCaMP5 (green) and DAPI nuclear (blue) signals in a confocal reconstruction tiling a fixed sagittal brain slice from a mouse injected in the APC with AAV2.9 *GCaMP5*-expressing viruses. Bottom: insets for APC (left), anterior olfactory nucleus (AON) (center), and OB (right); GL, glomerular layer; EPL, external plexiform layer; MCL, mitral cell layer; GCL, granule cell layer; A, anterior; P, posterior; D, dorsal; V, ventral.

(D) Example field of view \sim 300 μ m deep from surface of GCaMP5 labeled cortical feedback axons and boutons in an awake head-fixed mouse.

(E) Spontaneous activity traces (dF/F₀) from feedback boutons marked in (D). Top six traces and respectively bottom four traces are from boutons of two different axonal branches.

(F) Histogram of pairwise correlations of baseline activity (dF/F) in a 3 min interval preceding odor presentation; green and black traces corresponds to bouton pairs from different and respectively same axonal branches.

(G) Pairwise correlations of baseline activity (dF/F) in a 3 min interval preceding odor presentation as a function of spontaneous events frequency; shaded area corresponds to standard deviation.

(H) Odor responses of four example boutons in GCL across four different stimuli (hexanal, acetal, [S]-limonene, ethyl tiglate, 0.4% saturated vapor pressure). Individual repeats (gray) and average traces (black) are shown; odors trigger both positive (enhanced responses) and negative (suppressed responses) deflections from baseline; * marks significant odor responses; stimulus duration, 4 s.

(I) Average fraction of cortical feedback boutons imaged responsive to odor (Odor) and APC electrical stimulation (Electrical) (40 pulses, 100 μ s, at 100 Hz, 30 μ A); error bars indicate SEM calculated over odors and fields of view (left) and fields of view respectively (right).

(J) Histogram of the number of odors in the panel (Odor Set A, Table S1) that individual feedback boutons in the GCL responded to.

fluorescence distribution; [Figures S2C–S2F](#); see [Experimental Procedures](#)). Odor presentation triggered significant responses in ~35% of all imaged boutons (responsive to at least one odor, [Figure 1H](#)). A given odor in the panel (Odor Set A, [Table S1](#)), on average, triggered responses in only $4.3\% \pm 0.4\%$ ($N = 20$ odors) of cortical feedback boutons imaged in the GCL (5,221 boutons, 18 FOVs, 4 mice), and on average a bouton responded to 0.85 ± 0.03 odors ([Figures 1I and 1J](#)). Within the subset of responsive boutons, individual boutons responded sparsely (2.5 ± 0.07 , odor responses/bouton, $N = 1,827$ responsive boutons) through enhancement (~45%) and more often suppression (~55%) of baseline activity (4,412 odor-bouton pairs, 4 mice, [Movies S2 and S3](#)). The distribution of number of odor responses per bouton did not follow a single binomial distribution, suggesting the presence of distinct populations of highly selective, as well as more promiscuous feedback boutons ([Figures S2G and S2H](#)).

A direct comparison of activity patterns from the same boutons across anesthetized and awake conditions showed significant reduction in spontaneous events during anesthesia (ketamine/xylazine, see [Experimental Procedures](#), 4.6 ± 0.4 spontaneous events per 3 min interval versus 10.2 ± 0.5 , $N = 283$ boutons, 2 mice, $p < 0.001$, Wilcoxon signed-rank test; [Figures S3A and S3B](#)). Suppressed odor responses were weaker under anesthesia ([Stettler and Axel, 2009](#)) (~84% of suppressed responses were weaker, $N = 112$, $p < 0.001$, Wilcoxon signed-rank test; [Figure S3C](#)). Enhanced responses showed both increases and decreases in response amplitude and number of responsive boutons under anesthesia ($N = 326$ bouton-odor pairs, 2 mice; [Figures S3C and S3D](#)), and on average were stronger ([Figure S3C](#)) and more robust across trials (SD / mean response = 1.2 ± 0.09 awake versus 0.72 ± 0.09 anesthetized, $p < 0.001$, Wilcoxon signed-rank test). In anesthetized mice, a given odor triggered responses in an average of $7.42\% \pm 0.22\%$ of imaged feedback boutons in the GCL ($N = 326$ responsive bouton-odor pairs, 2 mice), similar in range to reports monitoring responses in cell bodies from the piriform cortex ([Stettler and Axel, 2009](#)). Corticalbulbar feedback activity depends heavily on the brain state. Thus, for the rest of this study, we restricted experiments to awake, head-fixed mice.

To determine whether the sparse nature of observed feedback odor responses can be accounted for by poor cell health (from viral GCaMP5 expression) or limited sensor sensitivity, we electrically stimulated the APC ($8 \times 100 \mu\text{s}$ pulses, 100 Hz, $30 \mu\text{A}$, see [Experimental Procedures](#)) while monitoring feedback responses. Electrical stimulation evoked strong and long-lasting calcium transients in the majority of boutons (85%; [Figure 1I](#); [Figures S4A and S4C](#)), likely due to dense recurrent connections in the APC ([Franks et al., 2011](#)).

To assess the relationship between neuronal spike rate and fluorescence measurements, we similarly monitored the change in GCaMP5 signals in corticalbulbar feedback boutons in response to electrical stimulation in the APC ($100 \mu\text{s}$, $50 \mu\text{A}$, see [Experimental Procedures](#)) of awake mice. To eliminate the contribution of intra-cortical recurrent activity to the GCaMP5 responses, we performed these experiments in conjunction with local injection of the GABA_A receptor agonist muscimol in the APC (0.5 mg/ml, $1 \mu\text{l}$ over 5 min, see [Experimental Procedures](#)).

Using fluorescent muscimol (1.0 mg/ml, $2 \mu\text{l}$ over 10 min, see [Experimental Procedures](#)), in a subset of experiments ($N = 3$ mice), we confirmed that muscimol spread was restricted to the APC and did not diffuse to nearby cortical areas such as the AON (see [Experimental Procedures](#); [Figures S5B and S5C](#)). Muscimol injection significantly decreased the frequency of spontaneous events ([Figures S5D and S5E](#)) in cortical feedback boutons and completely abolished odor-evoked bouton responses ([Figure S5F](#)).

In the presence of muscimol, single pulses ($100 \mu\text{s}$, $50 \mu\text{A}$, see [Experimental Procedures](#)) failed to evoke calcium transients, suggesting that GCaMP5 activity may not report single action potentials ([Akerboom et al., 2012](#)). However, pairs of pulses, as well as stronger stimulation protocols did evoke detectable fluorescence transients ([Figures S5G and S5H](#)) with response kinetics matching reports from cultured neurons (~120 ms onset, ~250 ms offset, [Figures S5G, S5J, and S5K](#)). The amplitude of evoked calcium transients (dF/F) increased monotonically with the number of pulses per stimulation event (2–16 pulses at 50 Hz or 100 Hz) and spanned the range of dF/F values observed for bouton odor responses ([Figure S5H](#)).

Pyramidal neurons in the piriform cortex have been reported to fire spontaneous bursts of 2–5 spikes at high frequency (≥ 100 Hz) ([McCollum et al., 1991](#)). Spontaneous calcium transients in our data ([Figures 1E and S1H](#)) match the increase in fluorescence amplitude triggered by electrical stimulation bursts (2–16 pulses at 50 or 100 Hz, [Figure S5H](#)). These observations suggest that calcium transients observed in the corticalbulbar boutons, at rest, represent short bursts of several action potentials and may indeed reflect the ongoing spontaneous activity of pyramidal APC neurons.

To estimate the relationship between decreases in fluorescence during odor-evoked suppression and changes in neuronal firing rate, we obtained an estimate of the expected baseline bouton fluorescence given various rates of spontaneous activity. To this end, we convolved the average dF/F bouton response to APC electrical stimulation in the presence of muscimol (2 pulses, $100 \mu\text{s}$, $50 \mu\text{A}$, 100 Hz) with Poisson pulse trains of different frequencies ([Figure S5I](#)). We found that the amplitude of odor-suppressed responses was consistent with the fluorescence change calculated from a simulated average spike rate of a few Hz ([Figure S5I](#)), suggesting that the suppression in bouton fluorescence may reflect the silencing of spontaneous firing bouts in the APC ([Zhan and Luo, 2010](#)).

Two Distinct Corticalbulbar Feedback Channels: Enhanced versus Suppressed Boutons

Strikingly, boutons showed high selectivity in their mode of response (enhancement versus suppression). Approximately 40% of the responsive boutons reacted to odors exclusively by enhancement and 55% by suppression of their baseline activity ([Figures 2A–2D](#)). This dichotomy in response was present throughout the population, and became even more apparent when the analysis was restricted to boutons that were responsive to more than half of odors in the panel (0 out of 52 boutons showed mixed responses). The sparse nature and segregation of enhanced and suppressed responses remained apparent even when sampling a larger odor panel (33 odors, Odor Set B,

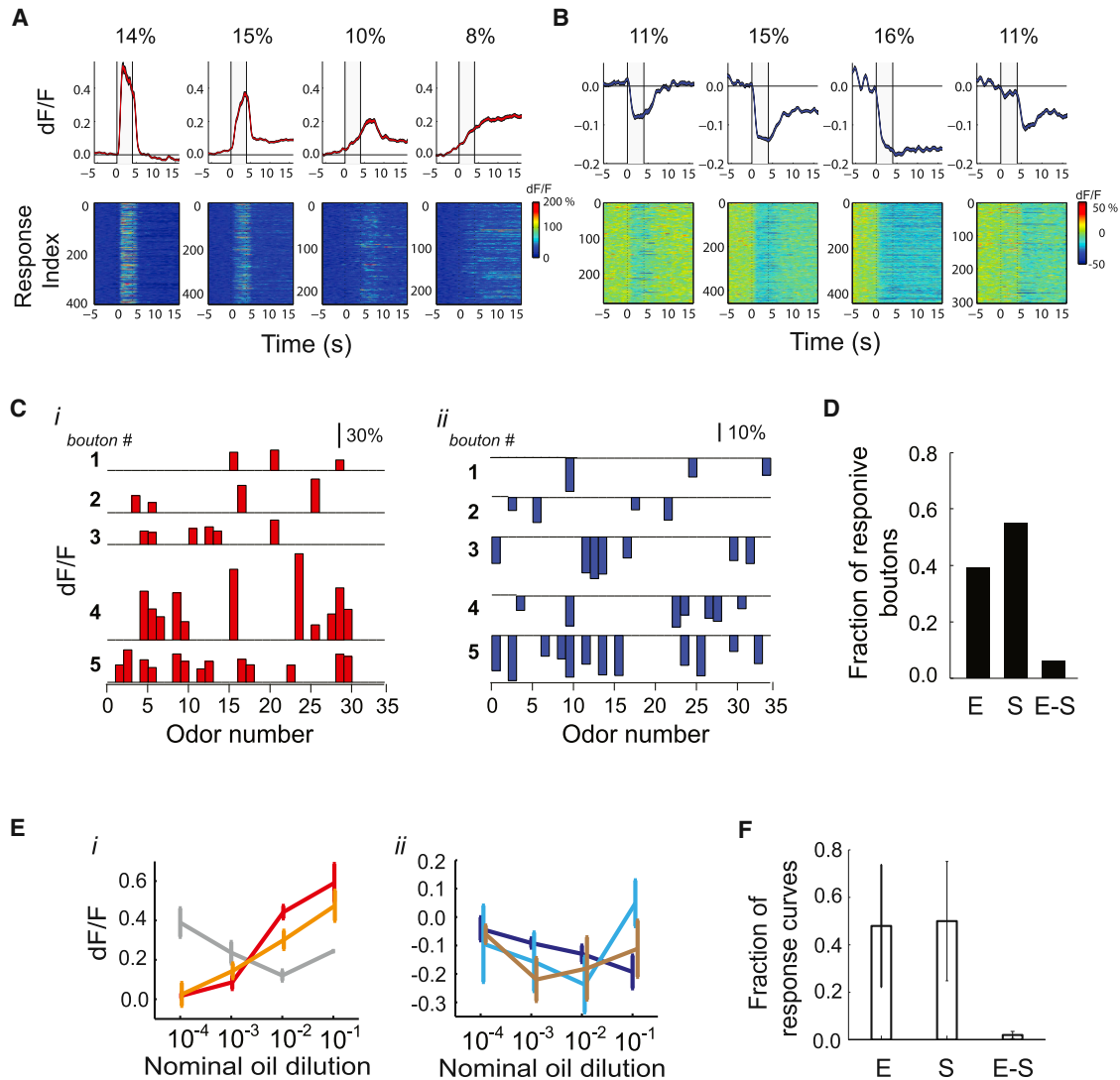


Figure 2. Dichotomy in Corticalbulbar Feedback Odor Responses: Enhanced versus Suppressed Boutons

(A and B) Odor response types obtained via k-means clustering and their relative distribution in the population of feedback boutons targeting the GCL; average response shapes (top) and all corresponding odor responses (GCaMP5) assigned to each cluster (bottom). (A) Enhanced response clusters; (B) suppressed response clusters.

(C) Example average odor response spectra (ORS) of enhanced (red) and suppressed (blue) boutons; sparsely responding boutons, as well as broadly tuned boutons are shown for illustration.

(D) Fraction of boutons responsive to odors in the panel (Odor Set A, Table S1) via only enhancement (E), only suppression (S), and both enhancement and suppression (E-S);

(E) Enhanced (i) and suppressed (ii) concentration-response (GCaMP5) curves for two odors (ethyl valerate, i, and heptanal, ii) in three example cortical feedback boutons; error bars indicate SEM across repeats.

(F) Fraction of concentration response curves that were purely enhanced (E), only suppressed (S), or showed both enhancement and suppression compared to baseline within the sampled concentration range (E-S); error bars indicate SD across fields of view.

Table S1; ~6.7% of responsive boutons showed both enhanced and suppressed responses, $N = 856$ boutons, 2 mice; Figure 2C, Figure S4D) and could not be easily explained by odor sampling biases. On average, suppressed boutons were as narrowly tuned to odors as enhanced boutons (average lifetime sparseness suppressed boutons = 0.60 ± 0.30 SD, $N = 849$ boutons versus 0.60 ± 0.23 SD, $N = 849$ enhanced boutons, $p = 0.95$, Wilcoxon rank-sum test). Furthermore, boutons belonging to the

same axon consistently showed either enhanced or suppressed odor responses (only 1 out of 52 analyzed axons had mixed responses), suggesting that the polarity of response segregates along different axons.

Suppressed boutons were more active in the baseline period (0.017 ± 0.001 events/s versus 0.010 ± 0.001 events/s, $p < 0.001$, t test) and displayed higher resting fluorescence (F_0) compared to enhanced boutons (Figures S4E–S4G). The lack

of excitatory odor responses in these boutons may simply result from baseline saturation of the GCaMP5 sensor. Conversely, the absence of negative deflections in the “enhanced” boutons could be explained by an intrinsic bias in calcium imaging methods toward detecting increases in fluorescence, given low resting activity. However, several pieces of evidence render these possibilities unlikely (Supplementary Note 1, Experimental Procedures, Figures S4E–S4H). In addition, we directly tested whether boutons suppressed by odors can in principle show an increase in their baseline fluorescence levels via APC electrical stimulation (see Experimental Procedures). Brief electrical stimulation (100 μ s at 30 μ A) during periods of odor-triggered suppression reliably resulted in increased fluorescence, switching the response polarity of individual boutons from suppression to enhancement (Figures S4A–S4C). This robust fluorescence increase upon electrical stimulation (Figure 1I) confirms that the observed dichotomy of suppressed and enhanced bouton odor responses is not an artifact of sensor saturation and may instead represent different selective populations of pyramidal cells in the APC that respond to odors mostly via enhancement or via suppression.

Corticalbulbar Feedback Responses Often Outlast Stimulus Presentation

Clustering of odor responses (see Experimental Procedures) revealed diverse temporal dynamics of both enhanced and suppressed bouton responses, including “transient,” “ramping,” “persistent,” and “lingering” features (Figures 2A and 2B, 18 FOV, 4 mice, 2,913 odor-bouton pairs). On average, enhanced responses tracked stimulus dynamics and changes in concentration more closely. Many boutons showed long-lasting activity patterns that outlasted the odor stimulus (4 s) by several seconds (>12 s) (76% of suppressed boutons, 35% of enhanced boutons). Further, $\sim 20\%$ of both suppressed and enhanced responses were triggered by the termination of odor stimulation (OFF responses). Given the GCaMP5 faster response kinetics (Figures S5G, S5J, and S5K), these observations indicate that brief odor inputs can initiate long-lasting bouts of activity in cortical feedback fibers which may further impact bulbar dynamics during fluctuating odor plumes or across multiple encounters of the same stimulus.

Separation of Enhanced and Suppressed Bouton Responses Is Maintained across Odor Concentrations

We investigated whether the dichotomy of bouton response types is particular to the odor concentrations used, or present across a wider range of stimulus intensities. Computational (Kaplan and Lansner, 2014; Wilson and Sullivan, 2011) and experimental (Franks et al., 2011; Stettler and Axel, 2009) studies in anesthetized mice have suggested that the piriform cortex shows invariance to changes in odor concentration. We sampled odor concentration (Figure 2E; Figures S6A and S6B; see Experimental Procedures) across ~ 3 orders of magnitude (Figure S6A). Only 10% of bouton responses were concentration invariant (changed average response amplitude across concentrations within the range of inter-trial variability, see Experimental Procedures; Figure S6C; 309/4,940 boutons, 6,582 bouton-concentration responses, 12 FOVs, 3 mice). Varying stimulus strength

modulated both the amplitude and number of bouton responses (Figure 2E; Figure S6). Across concentrations, some boutons showed monotonic increase/decrease in response amplitude, while others ($\sim 50\%$) followed complex non-monotonic response curves (see Experimental Procedures; Figures S6D–S6F). Importantly, within the sampled concentration range, we rarely ($<5\%$) observed a change in the response of the feedback boutons targeting the GCL from enhanced to suppressed and vice-versa (Figure 2F).

Differential Cortical Feedback Dynamics across Bulb Layers

In addition to targeting the GCL, corticalbulbar feedback fibers synapse sparsely on inhibitory interneurons in the glomerular layer (GL) as well (Figures 1C and 3A; Figures S1C and S1D). We tested whether the activity patterns and spatial organization of cortical feedback vary across bulb layers. Feedback boutons in the GL appeared to have more spontaneous activity compared to the ones in GCL (average = 14.9 ± 0.2 events per 3 min, $N = 3,355$ boutons, 10 FOVs, 6 mice versus 1.62 ± 0.1 , $N = 5,067$, 14 FOVs, 4 mice; Figure 3B; Figure S7A). A possible explanation for this discrepancy is the increased optical access to the superficial glomerular layer compared to the deeper granule cell layer. This apparent increase in baseline fluorescence can in principle facilitate the detection of suppressed odor responses. However, the GL feedback boutons were sparser in their responses (Figures 3C and 3D) compared to the deeper layers (average lifetime sparseness = 0.72 ± 0.23 SD, $N = 558$ responsive boutons in GL versus 0.61 ± 0.27 SD, $N = 1,527$ boutons in GCL, within same animals, $p < 0.001$, Wilcoxon rank-sum test). Specifically, purely suppressed boutons were significantly narrower in their tuning compared to their counterparts in the GCL (average lifetime sparseness = 0.81 ± 0.21 SD, $N = 296$ boutons in GL versus 0.60 ± 0.21 SD, $N = 849$ boutons in GCL, $p < 0.001$, Wilcoxon rank-sum test), while the enhanced boutons were matched in broadness of tuning across layers (average lifetime sparseness = 0.61 ± 0.21 SD, $N = 228$ GL boutons versus 0.60 ± 0.23 SD, $N = 632$ GCL boutons, $p = 0.86$, Wilcoxon rank-sum test; Figures 3C and 3D). Mixed boutons were a minority in the GL as well, but appeared more frequently compared to the GCL (14% E-S; Figure S7B). Clustering revealed several types of odor responses across the population, similar to those observed in the GCL with a significant fraction of responses outlasting stimulus offset ($\sim 48\%$ of suppressed, $\sim 34\%$ of enhanced responses, Figures S7C and S7D). Thus, across bulb layers, cortical bulbar feedback fibers differ in the frequency of suppressed responses but are similar in the presence of enhanced-suppressed bouton dichotomy and long-lasting responses.

Local Diversity in Cortical Feedback Representations across Odors

To determine whether cortical feedback is locally tuned or spatially distributed, we computed the degree of overlap in the odor responses of pairs of nearby and distant boutons monitored simultaneously. We first investigated the relationship between similarity of odor response spectra (correlation coefficient) and physical separation in the GCL boutons (Soucy et al., 2009).

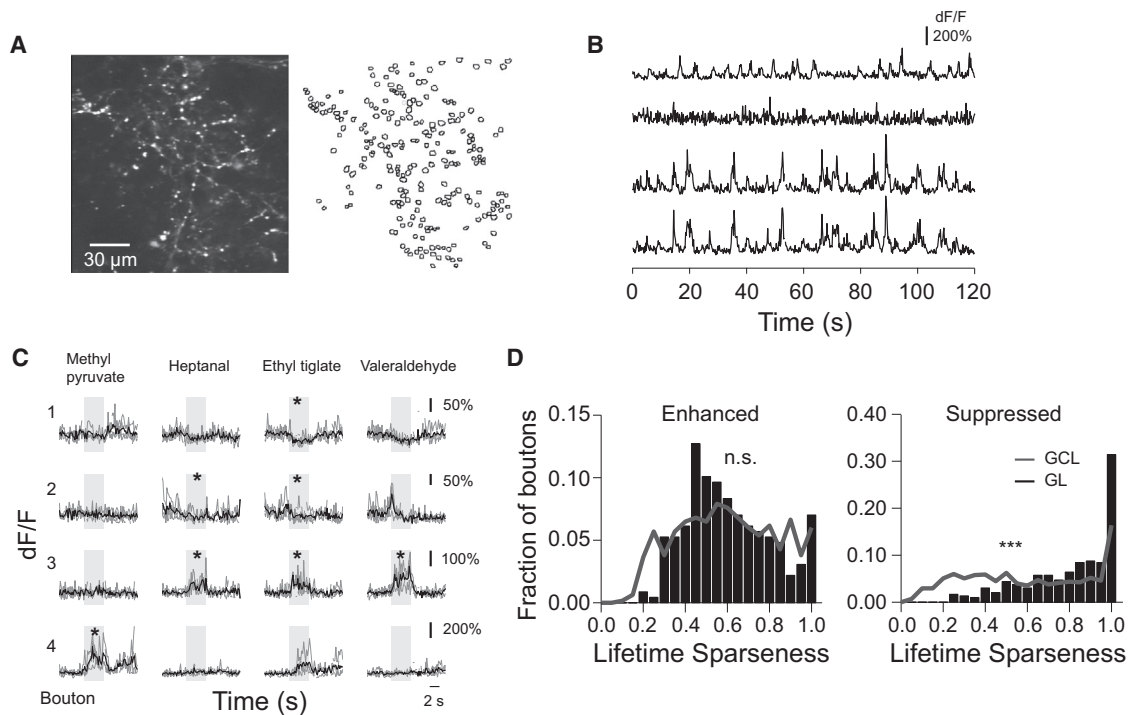


Figure 3. Differential Cortical Feedback Bouton Odor Responses across Bulb Layers

(A) Left: example field of view $\sim 80 \mu\text{m}$ deep from surface of GCaMP5 labeled cortical feedback axons and boutons in an awake head-fixed mouse; right: outlines of the regions of interest (ROIs) corresponding to putative cortical feedback boutons.

(B) Spontaneous activity traces from the feedback boutons selected in the field of view showed in (A). Bottom two traces correspond to boutons assigned to the same axonal branch by reconstruction of single axons.

(C) Odor responses of four example boutons in GL across four different stimuli (ethyl pyruvate, heptanal, ethyl tiglate, valeraldehyde, 0.4% saturated vapor pressure). Individual repeats (gray) and average traces (black) are shown; odors trigger both positive (enhanced responses) and negative (suppressed responses) deflections from baseline; * mark significant odor responses; stimulus duration, 4 s.

(D) Lifetime sparseness of boutons responsive to odors in the panel (Odor Set A, Table S1) only via enhancement (left) or suppression (right); distributions in the GCL (black bars) and GL (gray trace) are shown.

Pairwise analysis of simultaneously imaged boutons revealed low spontaneous correlations (average similarity = 0.06 ± 0.0003 , $N = 80,104$ bouton pairs; Figure S7E), as well as rich local diversity in response across odors (average similarity = 0.11 ± 0.001 , $N = 117,352$ pairs; Figures 4A and 4C). We observed a small excess of similarly responding boutons within $20 \mu\text{m}$ separation (Figure 4C; see Experimental Procedures), which can be explained by local enrichment in boutons belonging to the same axon (average distance between boutons anatomically identified on the same axon = $19.5 \pm 1.6 \mu\text{m}$). Beyond this small excess, no spatial order was apparent in bouton responses within the imaged field of view, implying that nearby boutons were as diverse in their responses as far apart ones ($<150 \mu\text{m}$, Figure 4C).

Are corticalbulbar feedback responses in the superficial layer organized according to the modular architecture of glomeruli? Within an example field of view, we found that nearby boutons may have very different odor response tuning. Indeed, pairwise comparisons of spontaneous activity ($\sim 63,500$ pairs, $N = 10$ FOVs, 6 mice) and odor response spectra ($\sim 27,500$ pairs, $N = 6$ fields of view, 4 mice) of bouton pairs showed low correlation across boutons in close proximity of each other, as well as across different fields of view ($<150 \mu\text{m}$ separation, average

spontaneous similarity = 0.04 ± 0.0003 , average odor similarity = 0.06 ± 0.001 ; Figures 4B and 4D; Figure S7F). Similar to the GCL, beyond a small excess of similar boutons within $20 \mu\text{m}$ separation, no obvious spatial organization was observed. Our results suggest that cortical feedback is distributed, locally heterogeneous, and matches the functional diversity observed for example in the responses of some of its potential GC targets (H.C. and D.F.A, unpublished data). These findings contrast previous spatial functionally tuned models of the OB (Johnson and Leon, 2007; Sallaz and Jourdan, 1993; Uchida et al., 2000; Willhite et al., 2006) and are consistent with recent reports of local diversity of glomerular inputs (Ma et al., 2012; Soucy et al., 2009).

We identified two distinct feedback bouton types, strikingly different in the polarity of their odor responses. We set to investigate whether they represent independent channels conveying information from the cortex to the sensory periphery or are redundant in the nature of their odor representations. Within each field of view, for each odor, we assembled a response vector containing the response amplitudes (average dF/F) of all anatomically selected boutons (see Experimental Procedures). We computed the pairwise odor similarity for stimuli within our panel in terms of overlap in their response vectors considering

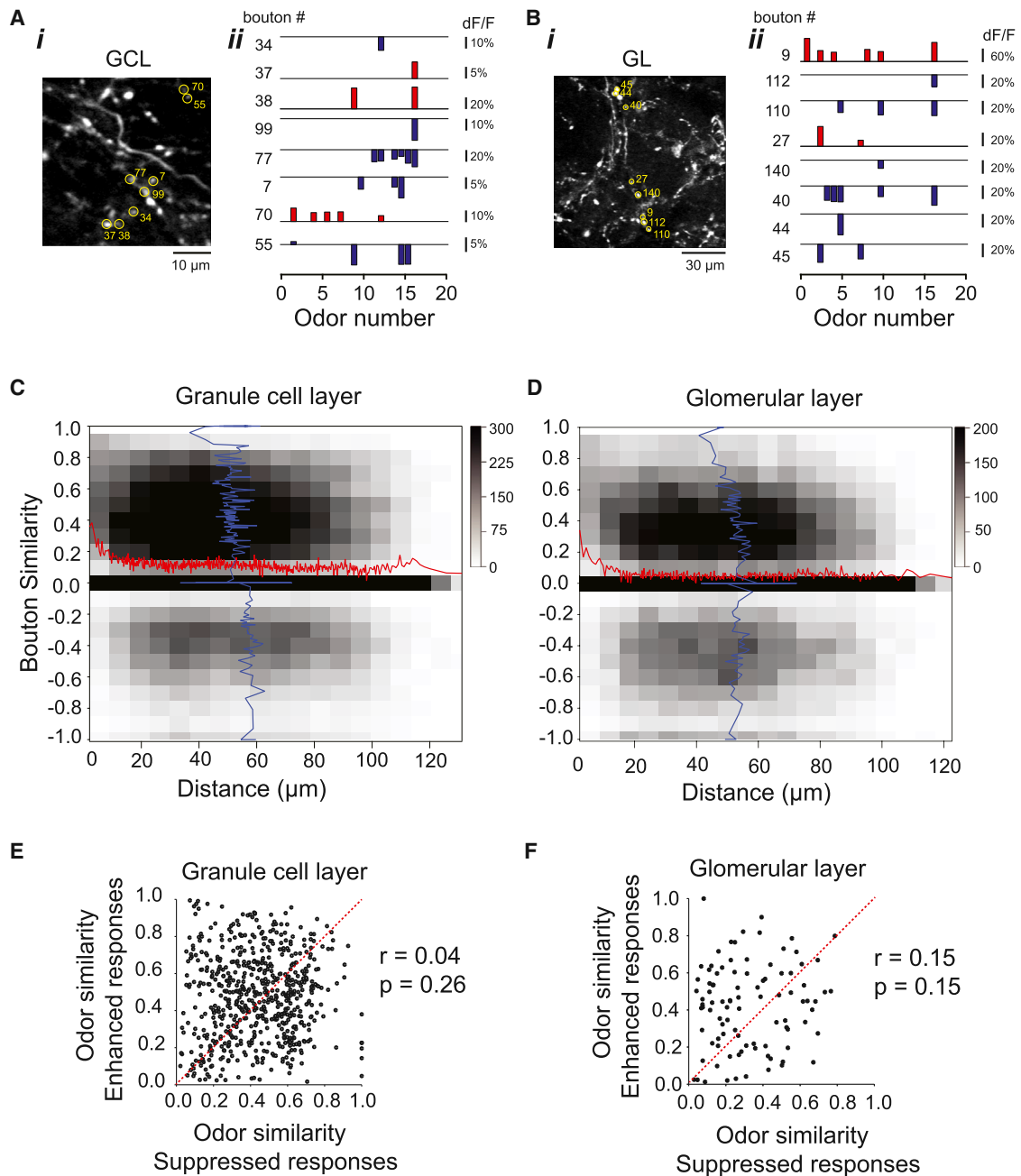


Figure 4. Cortical Feedback Representations Are Locally Diverse

(A and B) Left: example fields of view $\sim 250 \mu\text{m}$ (A) and $\sim 80 \mu\text{m}$ (B) from OB surface of GCaMP5-labeled cortical feedback axons and boutons in an awake head-fixed mouse; center: odor response spectra (ORS) of eight example boutons marked in the fluorescence image.

(C and D) Two-dimensional histogram of pairwise correlations between ORS (Odor Set A, Table S1) of individual boutons in the granule cell layer (C) and glomerular layer (D) versus their physical separation. Red, average similarity (pairwise correlation) across different inter-bouton distances; blue, average inter-bouton distance across all similarity values of bouton pairs; grayscale, number of pairs per bin.

(E and F) Odor similarity in terms of only enhanced versus only suppressed bouton responses in the granule cell (E) ($r = 0.04$) and glomerular layers (F) ($r = 0.15$); numbers indicate the Pearson's linear correlation coefficient (r) and the associated p values, calculated using a paired t test.

either enhanced responses, or suppressed responses only, respectively. If the average similarity value for an odor pair obtained using the enhanced responses only is predictive of the corresponding value calculated using suppressed responses,

then plotting them against each other should result in a cloud of points distributed along a line, with the amplitude and diversity of residuals indicating deviations from this scenario. In both GCL and GL, we did not observe significant correlations between the

two representations (for GCL, $r = 0.04$, $p = 0.27$, $N = 615$ odor pairs; for GL, $r = 0.15$, $p = 0.15$, $N = 99$ odor pairs, *t* test; [Figures 4E and 4F](#)). We computed the mutual information between the similarity in odor representations given by enhanced and suppressed boutons (see [Experimental Procedures](#)). We found no significant interdependence between the enhanced and suppressed odor representations in the GL (0.68 bits versus 0.76 ± 0.1 SD bits, shuffled control, $p = 0.9$), and only small (but statistically significant compared to shuffled control) dependence in GCL (0.21 bits versus 0.16 ± 0.01 SD bits, $p < 0.01$). Thus, the enhanced and suppressed boutons may represent two distinct piriform cortex output channels, which are relayed back to the sensory periphery.

Cortical Feedback Sparsens Odor Representations and Decorrelates Mitral, but Not Tufted Cell Responses

How does corticalbulbar feedback influence OB output? Our experiments indicate that odors enhance and suppress cortical feedback to the bulb. Hence, in principle, cortical feedback can either inhibit or disinhibit MT cells, via differential regulation of interneuron activity. Therefore, to directly determine the contribution of cortical feedback in shaping MT cell odor responses, we turned to loss-of-function manipulations via pharmacological suppression of activity in the APC. Cortical activity was suppressed by injection of the GABA_A receptor agonist muscimol (fluorescent or non-fluorescent, see [Experimental Procedures](#)) through chronically implanted cannulae into the APC (for fluorescent muscimol, ~ 1 mm A-P and ~ 0.5 mm M-L, size bolus, $N = 3$ mice; [Figures S5A–S5C](#)) resulting in complete silencing of bouton odor responses ([Figures S5D–S5F](#)).

We analyzed the effects of cortical silencing on the activity of mitral (MC) and tufted cells (TC) using multiphoton imaging of GCaMP3.0 signals. We used genetically engineered *TBET*-Cre mice crossed to a GCaMP3.0 reporter line (Al38, Allen Brain Institute; [Zariwala et al., 2012](#)) to ensure spatially homogeneous expression of the calcium sensor in MT cells ([Haddad et al., 2013](#)). Mitral cells were differentially identified from tufted cells by their denser packing, larger soma size and depth from surface ([Figure 5A](#) versus [6A](#)). We observed an increase in the amplitude of response, as well as in the number of odor-responding mitral cells ([Figures 5A–5E](#); [Figures S8A](#) and [S8B](#); [Movie S4](#)), accompanied by a significant loss of odor selectivity upon muscimol injection (average number of odor responses per cell = 8.37 ± 0.35 pre-muscimol versus 13.92 ± 0.49 post-muscimol, $N = 465$ MCs, 6 hemibulbs, Wilcoxon signed-rank test, $p < 0.001$; [Figure 5F](#)). We verified that saline injections did not change mitral cell responses (average number of odor responses per cell = 7.32 ± 0.41 pre-saline versus 6.99 ± 0.35 , post-saline $N = 333$ cells, 4 hemi-bulbs, Wilcoxon signed-rank test, $p = 0.12$; [Figure 5D](#); [Figure S8D](#)). A similar trend was observed in average lifetime sparseness quantifications ([Figure 5G](#); [Figure S8F](#)).

Consistent with previous reports ([Nagayama et al., 2004](#)), we found that tufted cells were more responsive than mitral cells for a given panel of odors, both in amplitude and number of odor responses per cell ([Figures 6A–6C](#)). Suppression of APC activity had substantially milder effects on the amplitude and number of responsive TCs ([Figures 6D](#) and [6E](#)). In comparison to the effect on MCs, muscimol injection did not significantly alter

the number of odor responses for a given TC (average number of odor responses per cell = 15.03 ± 0.49 pre-muscimol versus 14.59 ± 0.51 post-muscimol, $N = 309$ cells, 5 hemibulbs, Wilcoxon signed-rank test, $p = 1$; [Figure 6F](#); [Movie S5](#)) and only mildly affected TC lifetime sparseness ([Figure 6G](#)). No obvious changes were observed in saline injected controls (average number of odor responses per cell = 17.40 ± 0.52 pre-saline versus 15.63 ± 0.51 post-saline, $N = 233$ cells, 4 hemi-bulbs, Wilcoxon signed-rank test, $p = 1$; [Figures S8E](#) and [S8G](#)).

To quantify the effect of APC silencing on mitral and tufted response amplitude, we calculated for each cell the signed Euclidean distance from the diagonal unity line when plotting its response “post” versus “pre” muscimol injection. Increase in response amplitude post-injection will result in values greater than zero ([Figures 5E](#) and [6E](#), see [Experimental Procedures](#)). Silencing APC resulted in more robust potentiation of MC versus TC response amplitudes (average distance for MCs = 0.034 ± 0.0008 , $N = 7,528$ odor-cell pairs versus -0.006 ± 0.002 , $N = 5,662$ odor-TC cell pairs, Wilcoxon rank-sum test, $p < 0.001$, [Figures 5E](#), [6E](#), [6H](#), and [6I](#)). These differential effects between mitral and tufted cells were also reflected in a positive shift in a change index (CI, see [Experimental Procedures](#)) calculated to quantify the modulation of response amplitude (average CI for MCs = 0.26 ± 0.008 , $N = 7,538$ odor-cell pairs versus 0.02 ± 0.004 , $N = 5,662$ odor-TC cell pairs, Wilcoxon rank-sum test, $p < 0.001$).

We analyzed the effects of cortical suppression on the mitral and tufted cell population odor representations ([Figure 7A](#)). Muscimol injection significantly increased pairwise similarity (correlation) of odor response spectra (ORS) of simultaneously imaged mitral cells (calculated for signals averaged across repeats), compared to pre-muscimol baseline (average MC similarity = 0.18 ± 0.002 , pre-muscimol versus 0.49 ± 0.002 , post-muscimol, $N = 27,391$ mitral cell pairs, Wilcoxon signed-rank test, $p < 0.001$, [Figure 7B](#); [Figure S8C](#)). Importantly, this increase in pairwise correlation was significantly higher than a shuffled control (average shuffled MC similarity = 0.36 ± 0.002 , Wilcoxon signed-rank test, $p = 0$; see [Experimental Procedures](#); [Figure S8H](#)) and thus could not simply be explained by increases in the mitral cell odor response amplitude. No significant increase in MC pairwise similarity was observed in saline control experiments (average MC similarity = 0.17 ± 0.002 , pre-saline versus 0.15 ± 0.002 , post-saline, $N = 309$ cells, 19,329 MC pairs, 4 hemibulbs, Wilcoxon signed-rank test, $p = 1$). In contrast, we did not observe any significant change in the pairwise cell ORS similarity across TCs post muscimol injection (average TC similarity = 0.46 ± 0.002 , pre-muscimol versus 0.46 ± 0.002 , post-muscimol, $N = 309$ cells, 11,522 TC pairs, 5 hemibulbs, Wilcoxon signed-rank test, $p = 0.25$; [Figure 7C](#); [Figure S8J](#)). Further, scaling down the “post-muscimol” response magnitude by a constant factor (“downscaled muscimol”) to match the “pre-muscimol” mean response amplitude did not lead to significant correlation change when compared to the “post-muscimol” condition for neither MCs nor TCs ([Figures S8L](#) and [S8M](#)).

The higher-odor sensitivity and denser responses in TCs suggest that neuronal representations would be harder to separate on the basis of odor identity when considering TC as opposed to MC population odor responses. Indeed, a pairwise odor correlation analysis (see [Experimental Procedures](#)) indicated that

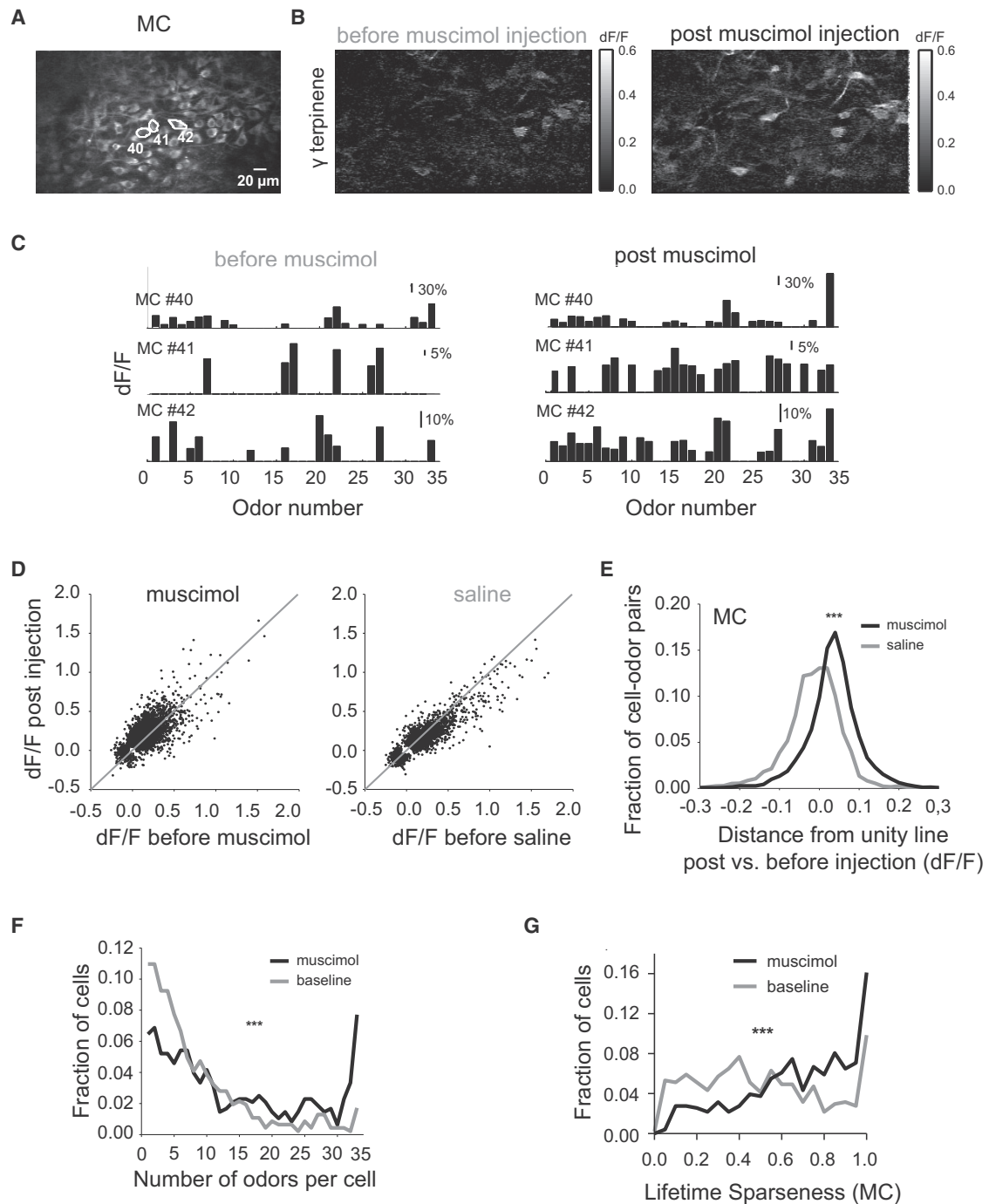


Figure 5. Suppression of APC Activity Increases Mitral Cell Responsiveness

(A) Average resting fluorescence of an example field of view in the mitral cell layer ($\sim 220 \mu\text{m}$ from surface).

(B) Ratio image (dF/F) showing average fluorescence change in response to γ terpinene in the field of view shown in (A) before (left) and after (right) muscimol injection.

(C) Example ORS (Odor Set B, Table S1) of three mitral cell bodies outlined in (A) before (left) and after (right) muscimol injection; each bar indicates the average response amplitude (dF/F) to a given odor in the panel.

(D) Scatter plots showing the odor induced change in mitral cell body fluorescence (dF/F) before and after muscimol (left) and respectively saline injection (right); each dot indicates the response of a cell to a given odor (cell-odor pair) before versus after injection; only cell-odor pairs that were detected as significant in at least one of the two conditions are shown; gray line marks slope of 1.

(legend continued on next page)

TC odor representations (Figure 7A) are more similar across odor stimuli compared to corresponding MC representations (average MC odor similarity = 0.26 ± 0.009 versus 0.49 ± 0.005 , $N = 528$ odor pairs for TC, 10 hemibulbs for MC and 9 hemibulbs for TC, Wilcoxon rank-sum test, $p < 0.001$; see [Experimental Procedures](#); [Figures 7D](#) and [7E](#)). In our experiments, more MCs than TCs were imaged simultaneously in a given field of view, which could account in principle for the lower odor similarity in the mitral cells population responses. However, pooling random subsets of cells per field of view, such as to obtain matching number of mitral and tufted cells for computing the odor similarity, reached the same conclusion as above (see [Experimental Procedures](#); [Figure S8N](#)). APC silencing resulted in a significant increase in odor similarity in the MC population representations (average MC odor similarity = 0.29 ± 0.01 pre-muscimol versus 0.45 ± 0.01 post-muscimol, $N = 528$ odor pairs, 6 hemibulbs, Wilcoxon rank-sum test, $p < 0.001$; see [Experimental Procedures](#); [Figure 7F](#); [Figure S8I](#)). In contrast, APC silencing had significantly milder effect on the TC odor representations (average TC odor similarity = 0.49 ± 0.005 pre-muscimol versus 0.53 ± 0.003 post-muscimol, $N = 528$ odor pairs, 5 hemibulbs, Wilcoxon rank-sum test, $p < 0.001$; [Figure 7G](#); [Figure S8K](#)). Interestingly, suppression of APC activity brought the odor similarity, as well as pairwise ORS similarity computed for MCs post-muscimol in the range of TC baseline (pre-muscimol) representations. No significant increase in odor similarity in the MC population responses was observed in saline control experiments (average MC odor similarity = 0.20 ± 0.006 , pre-saline versus 0.20 ± 0.005 , post-saline, $N = 528$ odor pairs, 4 hemibulbs, Wilcoxon signed-rank test, $p = 0.99$).

Taken together, our results show the existence of specific cortical feedback regulation of the odor representations of mitral versus tufted cells in awake mice. This form of top-down control differentially decorrelates mitral, but not tufted cell population responses, thus potentially enabling odor separation in subsequent olfactory areas.

DISCUSSION

We characterized the dynamics of corticalbulbar feedback projections in awake head-fixed mice across different bulb layers using multiphoton microscopy. Our results indicate that cortical feedback is odor specific, sparse, and layer selective and is routed via two distinct types of boutons which respond mostly with enhancement or suppression of baseline activity ([Figures 1](#), [2](#), and [3](#)). Feedback representations were locally diverse and often long lasting ([Figures 2](#) and [4](#)). Suppression of these feedback signals via pharmacological silencing of the piriform cortex differentially modulated the OB output, resulting in

decreased odor separation across populations of mitral cells, but not tufted cells ([Figures 5](#), [6](#), and [7](#)).

Corticalbulbar Feedback Is Routed through Distinct Channels of Enhanced and Suppressed Boutons

Previous work in the APC has described spatially distributed and sparse odor responses ([Miura et al., 2012](#); [Poo and Isaacson, 2009](#); [Stettler and Axel, 2009](#); [Zhan and Luo, 2010](#)). A study using intracellular recordings in APC of awake mice has reported equal distribution of sparse (responsive to 1 in 20 stimuli, ~50%) and broadly tuned (responding to half or more of sampled stimuli, ~50%) pyramidal cells. The broadly tuned cells were either predominantly excited (25%) or inhibited (25%) by odorants ([Zhan and Luo, 2010](#)). Our results show that responses of cortical boutons that project to the OB are largely sparse and odor selective ([Figure 1](#)), broadly tuned boutons representing only a small minority ([Figure 1I](#); [Figures S2G](#) and [S2H](#)). Further, irrespective of their tuning (lifetime sparseness), individual boutons fall into distinct types of “enhanced” and “suppressed” boutons based on their response mode. The differences in broadness of tuning between our observations and APC recordings may reflect anatomical biases in corticalbulbar projection patterns. Functional specificity in feedback projections emerging from primary cortical areas has been reported in the visual and somatosensory systems ([Glickfeld et al., 2013](#); [Jarosiewicz et al., 2012](#); [Sato and Svoboda, 2010](#); [Vélez-Fort et al., 2014](#)) and may represent a general feature across sensory modalities.

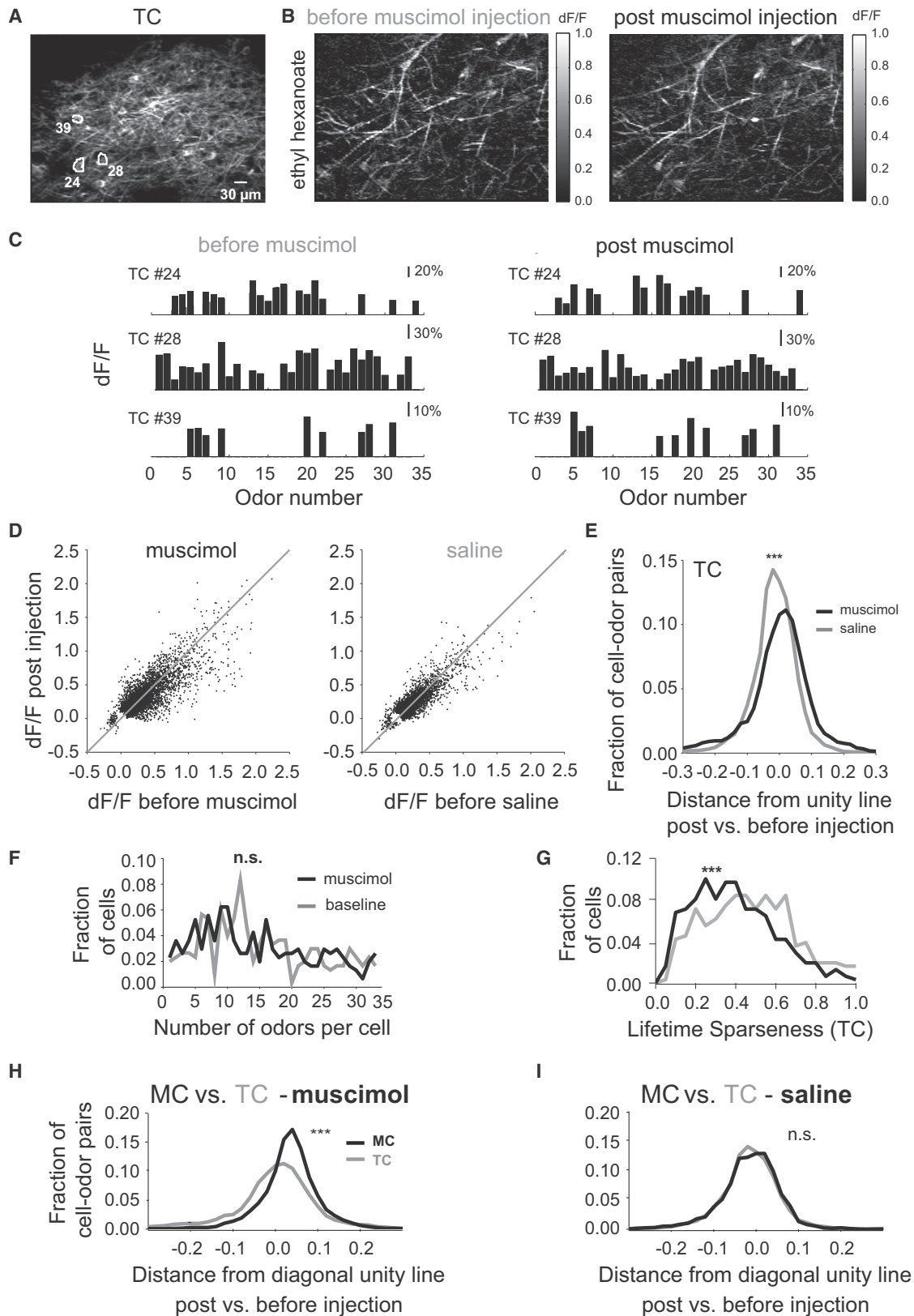
The functional dichotomy between enhanced and suppressed boutons segregated along axons and could not be explained by imaging artifacts, as indicated by electrical stimulation experiments ([Figures S4A–S4C](#)). Our finding is consistent with the existence of different populations of corticalbulbar projecting neurons that respond to odors mostly via enhancement or mostly through suppression. The dichotomy may arise from recurrent excitatory-inhibitory interactions within the APC itself ([Franks et al., 2011](#); [Suzuki and Bekkers, 2011](#); [Zhan and Luo, 2010](#)), via presynaptic modulation of cortical feedback fibers in the OB, or both. These models necessitate specific targeting of individual pyramidal neurons/fibers by regulatory circuits and our approach does not distinguish between them. Screening genetically identified classes of APC pyramidal neurons using intersectional strategies ([Fenno et al., 2014](#)) in future studies will provide insight into the underlying substrates and the differential effects of these feedback inputs on their OB targets.

Top-down cortical input to the bulb via distinct channels of enhanced and suppressed boutons may be key to increasing the flexibility of feedback action. In one scenario, differential enhancement and suppression may allow feedback to gate

(E) Summary histogram showing change in odor-evoked mitral cells responses upon muscimol (black) and saline (gray) injections compared to pre-injection baseline; the change for each mitral cell odor response (each dot in D is quantified as the Euclidian distance from the diagonal unity line; gray line indicating slope of 1).

(F) Histogram of the number of odors individual mitral cells responded to before (gray trace) and after (black trace) muscimol injection.

(G) Histogram of lifetime sparseness values for individual mitral cells before (gray trace) and after (black trace) muscimol injection (average lifetime sparseness = 0.68 ± 0.01 pre-muscimol versus 0.50 ± 0.01 post-muscimol, $N = 509$ MCs, 6 hemibulbs, Wilcoxon signed-rank test, $p < 0.001$); *** indicates significance level ($p < 0.001$, Wilcoxon signed-rank test).



(legend on next page)

specific subsets of OB interneurons and enhance discriminability of behaviorally relevant odors in a context-specific manner.

Cortical Feedback Responses Outlast Odor Stimuli and Are Locally Diverse

We found that feedback responses, especially in the suppressed boutons, often lingered for seconds, long after the end of stimulus presentation (Figure 2; Figure S7). These lasting signals could not simply be explained by slow calcium (reporter) dynamics or motion artifacts, as they were accompanied in the same field of view and same trial by transient responses in neighboring boutons and were preceded in the same boutons by fast spontaneous events during baseline period (Figures 1E and 3B). Also, electrical stimulation experiments demonstrated fast GCaMP5 dynamics (Figures S5G, S5J, and S5K). Persistent feedback responses have also been reported in other brain areas (Petreanu et al., 2012) and may constitute a short-term memory trace that binds recently elicited activity patterns in the APC to ongoing sensory inputs in the OB.

Importantly, responses of corticalbulbar feedback boutons were locally diverse, lacking apparent spatial modular organization both in the glomerular and granule cell layers (Figure 4). This is consistent with recent reports documenting the non-chemotopic organization and functional diversity of the bulbar circuitry (Soucy et al., 2009). Locally heterogeneous feedback inputs together with the long-lasting nature of the responses may allow individual bulbar neurons to integrate olfactory inputs both across a large space of neuronal representations, as well as in time, which are basic ingredients for reconstructing odor identity during active exploration.

Differential Decorrelation of Mitral but Not Tufted Cell Odor Representations by Cortical Feedback

The OB output is relayed to downstream areas via mitral and tufted cells. These two populations differ in anatomical location, response properties and projection patterns (Fukunaga et al., 2012; Igarashi et al., 2012; Nagayama et al., 2004, 2010) and may perform different functions: aiding odor detection versus

identification. Suppression of cortical activity had significantly different impact on mitral versus tufted cells (Figures 5, 6, and 7). This may partly arise from the differences observed in cortical feedback responses across the superficial and deep bulb layers (Figure 3). In the absence of feedback, we observed an increase in the similarity of mitral cell odor responses across the population (Figure 7). In contrast, pairwise response similarity across tufted cells showed no significant change. As a consequence, mitral cell population representations of different odors became more similar, suggesting a substantial loss in odor separability for downstream decoder circuits in the absence of corticalbulbar feedback.

Tufted cells intrinsically show higher excitability (shorter latency and stronger response amplitudes), stronger feedforward evoked excitation (Burton and Urban, 2014), and similarity in the odor responses compared to mitral cells. Tufted cells project in high numbers to the AON and olfactory tubercle and could also be differentially modulated by feedback originating from more anterior areas, such as the AON, and to lesser degree from the piriform cortex.

Our results suggest that, in addition to intrinsic biophysical and local connectivity differences between mitral and tufted cells, top-down cortical feedback is an essential ingredient for keeping these two OB output streams distinct from each other.

Decorrelation of ensemble neuronal responses in early sensory circuits has been proposed as a mechanism for separation of similar input patterns by downstream circuits (Laurent, 2002; Vinje and Gallant, 2000; Wiechert et al., 2010). The increased mitral cell correlations in the absence of cortical feedback could not be explained by an increase in mitral cell response amplitude (gain), as indicated by odor identity shuffling controls (Figure S8). Thus, the sparse and distributed cortical feedback does not simply downscale network activity in an unspecific manner, but helps redistribute activity across mitral cells and decorrelates their response patterns to aid odor separation. Our data are consistent with the view that cortical feedback acts specifically via interneurons in the OB, such as to sparsen odor representations at the level of MCs. Future experiments involving faster and

Figure 6. Suppression of APC Activity Only Mildly Alters Tufted Cells Responses

- (A) Average resting fluorescence of an example field of view containing tufted cell bodies and dendrites in the external plexiform layer (~140 μm from surface).
 (B) Ratio image (dF/F) showing average fluorescence change in response to ethyl hexanoate in the field of view shown in (A) before (left) and after (right) muscimol injection.
 (C) Example ORS (Odor Set B, Table S1) of three tufted cell bodies outlined in (E) before (left) and after (right) muscimol injection.
 (D) Scatterplots showing the odor-induced change in tufted cell body fluorescence (dF/F) before and after muscimol (left) and respectively saline injection (right); each dot indicates the response of a given cell to a given odor (cell-odor pair) before versus after injection; only cell-odor pairs that were detected as significant in at least one of the two conditions are shown; gray line marks slope of 1.
 (E) Summary histogram showing change in odor-evoked tufted cell responses upon muscimol (black) and saline (gray) injections compared to pre-injection baseline; the change for each mitral cell odor response (each dot in D is quantified as the Euclidian distance from the diagonal; gray line indicating slope of 1).
 (F) Histogram of the number of odors individual tufted cells responded to before (gray trace) and after (black trace) muscimol injection; Odor Set B, Table S1; n.s. indicates significance level ($p = 1$, Wilcoxon signed-rank test).
 (G) Histogram of lifetime sparseness values for individual tufted cells before (gray) and after (black) muscimol injection (average lifetime sparseness = 0.47 ± 0.01 pre-muscimol versus 0.39 ± 0.01 post-muscimol, $N = 308$ TCs, 5 hemibulbs, Wilcoxon signed-rank test, $p < 0.001$); Odor Set B, Table S1; *** indicates significance level ($p < 0.001$, Wilcoxon signed-rank test).
 (H and I) Summary histograms showing change in odor evoked mitral cell (black) and tufted cell (gray) responses upon muscimol (average distance for MCs = 0.034 ± 0.001 , $N = 7,538$ odor-cell pairs versus average distance for TCs = -0.006 ± 0.002 , $N = 5,662$ odor-cell pairs, Wilcoxon rank-sum test, $p < 0.001$) (H) and saline (average distance for MCs = -0.017 ± 0.001 , $N = 4,719$ odor-cell pairs versus average distance for TCs = -0.0157 ± 0.001 , $N = 3,047$ odor-cell pairs, Wilcoxon rank-sum test, $p = 0.56$) (I) injections compared to pre-injection baseline; the change for each cell odor response (each dot in Figures 5D and 6D) is quantified as the Euclidian distance from the diagonal (dotted line indicating slope of 1); *** indicates significance level ($p < 0.001$, Wilcoxon signed-rank test); n.s. indicates $p > 0.05$.

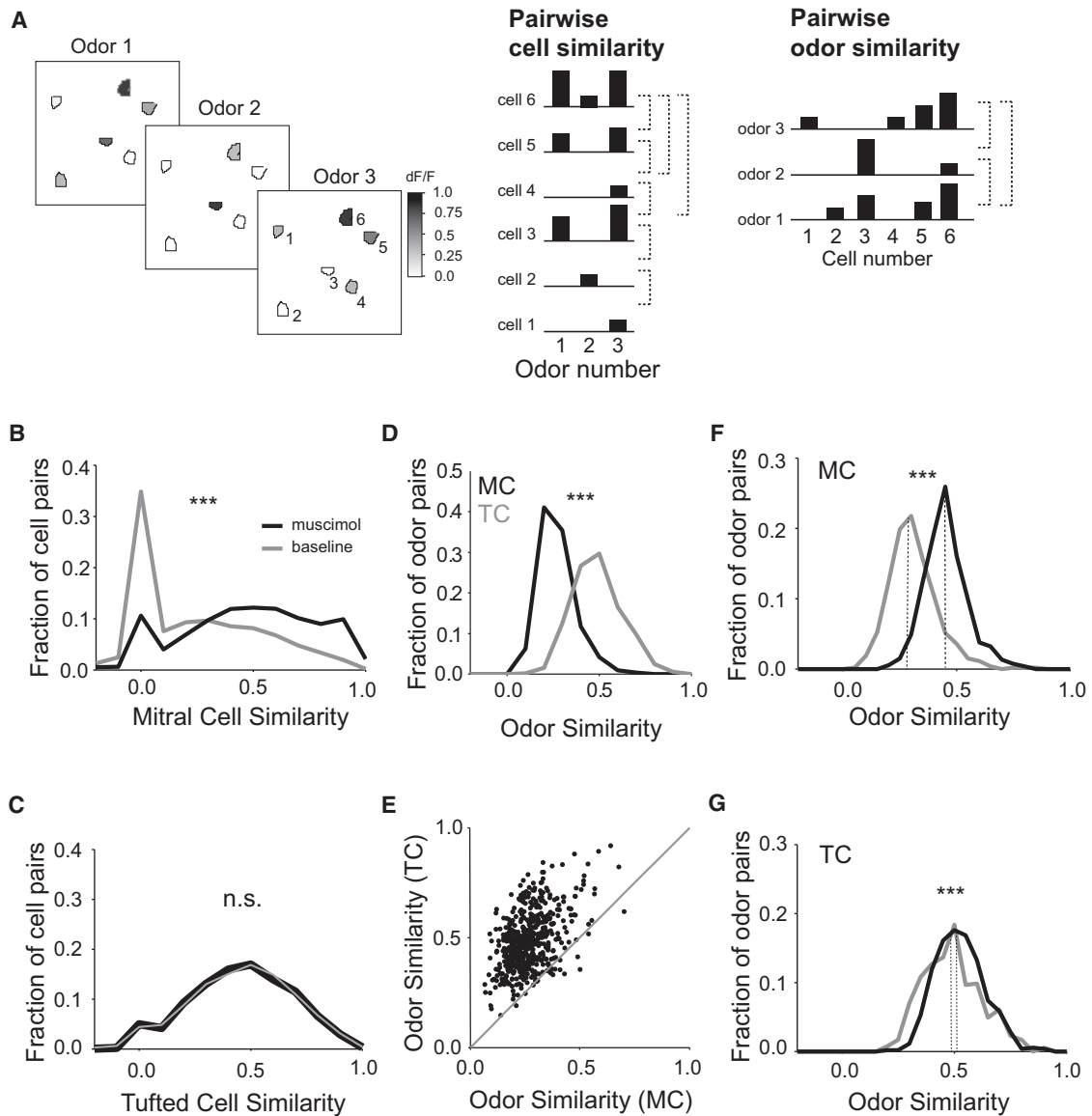


Figure 7. Suppression of APC Activity Decorrelates Mitral, but Not Tufted Cell, Odor Representations

(A) Schematic exemplifying pairwise cell similarity and pairwise odor similarity calculations for a given field of view; left: cartoon showing responses of six identified ROIs (black outlines) within a given field of view across three odors; colors indicate the average response amplitude (dF/F) for each ROI; center: an ORS is calculated for each ROI (cell) as the vector containing the average dF/F for each odor; pairwise cell similarity is calculated as the uncentered correlation between the ORS vectors for each pair of cells (indicated by dotted lines); right: a cell response spectrum (CRS) is calculated for each odor as the vector containing the average dF/F for each cell upon presentation of the given odor; pairwise odor similarity is calculated as the uncentered correlation between the CRS vectors for each pair of odors; Odor Set B, Table S1 used for (B)–(G).

(B) Histogram of pairwise cell similarity of mitral cells before (gray, baseline) and after (black) muscimol injection; Odor Set B, Table S1.

(C) Histogram of pairwise cell similarity of tufted cells before (gray, baseline) and after (black) muscimol injection; n.s. indicates significance level (p = 0.25, Wilcoxon signed-rank test).

(D) Histogram of pairwise odor similarity of mitral cells (black, MC) and tufted cells (gray, TC) before muscimol injection.

(E) Scatterplot of averaged pairwise odor similarity of mitral versus tufted cells before muscimol injection; each dot represents the comparison of average similarity scores for a given odor pair obtained from mitral and tufted cells odor representations across all sampled fields of view.

(F) Histogram of pairwise odor similarity of mitral cells responses before (gray) and after (black) muscimol injection; dotted lines indicate the median.

(G) Histogram of pairwise odor similarity of tufted cells responses before (gray) and after (black) muscimol injection; *** indicates significance level (p < 0.001, Wilcoxon signed-rank test); dotted lines indicate the median.

reversible methods (Boyd et al., 2012; Dhawale et al., 2010; Markopoulos et al., 2012) of suppressing activity, locally applicable in the OB, will help understand how the decorrelation of mitral cell outputs evolves over time and how it impacts odor discrimination speed and accuracy in behaving animals.

Our experiments characterizing the functional properties and spatial-temporal organization of corticalbulbar projections are a starting point in understanding how top-down signals originating in the piriform cortex guide olfactory processing. Monitoring the dynamics of corticalbulbar feedback and the consequences of targeted suppression of feedback fibers in animals analyzing varying odor signals in rich olfactory environments will advance our understanding of cortical feedback function during behavior.

EXPERIMENTAL PROCEDURES

All animal procedures conformed to NIH guidelines and were approved by Cold Spring Harbor Laboratory Institutional Animal Care and Use Committee. Detailed methods are available as [Supplemental Experimental Procedures](#). To express GCaMP5 in corticalbulbar axons, we anesthetized adult mice with ketamine/xylazine and injected them with a cocktail of AAV2.9 *Synapsin-Cre* and AAV2.9 *EF1-DIO-GCaMP5* in the APC at least 2 weeks before imaging. To gain optical access to the OB, we anesthetized animals, removed the bone over the bulb, and replaced it by a 3 mm coverslip (CS-3R, Warner Instruments). A titanium headbar was attached to the skull to fixate the animal during the imaging sessions. Mice were imaged using a Chameleon Ultra II Ti:Sapphire femtosecond pulsed laser (Coherent) coupled to a custom built multiphoton microscope.

Odor Delivery

Odors were presented in 4 s pulses, preceded by 10 s baseline and followed by 12 s recovery periods. Inter-trial intervals (ITIs) of at least 30 s were used between recording periods. During each ITI, a high air flow stream (>20 l/min) was pushed through the odor delivery machine to minimize odor contamination across trials. A serial air dilution odor machine was used to deliver odorized air (Odor Set A, [Table S1](#)) at 2.5 l/min rate at 0.4% saturated vapor pressure ([Figures 1D–1J](#), [2A](#), [2B](#), [2D](#), [3](#), and [4](#)). For experiments comparing bouton responses in awake versus anesthetized mice, as well as monitoring the effects of muscimol, a subset of 5 odors was used (acetal, hexanal, ethyl tiglate, ethyl caproate, and isoamyl acetate). A second, oil dilution-based odor machine (1 l/min rate; [Dhawale et al., 2010](#)) was used for experiments involving larger odor sets (1:100 mineral oil dilution, Odor Set B, [Table S1](#), for mitral and tufted cell imaging experiments, [Figures 5](#), [6](#), and [7](#)), and for probing concentrations (Concentration, [Table S1](#), 1:10⁴ to 1:10 nominal oil dilutions). Odor output was characterized using a photo-ionization device (Aurora Scientific) and calibrated in terms of concentration in air ([Figure S6A](#)). Odors in the panel were chemically diverse and activated glomeruli on the dorsal OB surface.

Data analysis

Image Registration

Images were registered using either the ImageJ plugin TurboReg (TurboReg) or via a previously described method ([Guizar-Sicairos et al., 2008](#)). The average registered image for each individual odor presentation was visually inspected to detect slow drifts in the z plane. Such instances were further discarded. ROIs were manually drawn for individual boutons (0.9–3 μm diameter) in ImageJ. For mitral and tufted cells imaging sessions, ROIs were manually selected based on anatomy (baseline average fluorescence). Care was taken to avoid selecting ROIs on cell bodies overlapping with neuropil (M/T lateral dendrites). To detect fast z movement on individual frames, we compared the shapes of each ROI in each frame with their corresponding averaged frames. Frames were a majority of ROIs changed shape were discarded from the analysis.

Spontaneous Activity, Assignment of Boutons, and Signal Detection

To detect spontaneous events, we estimated the distribution of resting fluorescence from the lower half of fluorescence values in the data. A fluorescence increase was called a spontaneous event if it exceeded the 99th percentile of the resting fluorescence. An ROI was considered spontaneously active if it showed at least two spontaneous events during a 3 min window. To determine whether two boutons belonged to the same axon, we visually inspected whether they appeared connected by an axonal segment in the imaged plane (337 “same axon” pairs, 52 axonal segments, and 648 “different axon” bouton pairs).

For each ROI and each odor presentation, the fluorescence signal across time was converted into dF/F values

$$(dF/F)_t = (F_t - F_o)/F_o$$

where, (dF/F)_t is the baseline subtracted, normalized fluorescence at time t; F_t is the instantaneous fluorescence at time t; and, F_o is the median fluorescence value during the initial air period.

Upon odor presentation, axonal boutons, mitral and tufted cells responded by increasing, and decreasing their fluorescence. ROI response to an odor presentation was quantified as the average dF/F over 4 s of odor presentation. To determine significance, we compared the odor evoked normalized fluorescence with values calculated during the air periods preceding all odor presentations in the session. Responses that exceeded the 99.9 percentile were called significantly *enhanced*. Responses that were below the 0.1 percentile were considered significantly *suppressed*. An ROI that showed significant responses to an odor in at least two repeats was considered *responsive* to that odor.

Concentration Invariance

Significance of each ROI for each odor response at each concentration was assessed independently. An ROI was classified as concentration invariant only if it cleared significance at all four concentrations used and the magnitude of responses did not differ across concentrations. To establish whether an ROI showed monotonically increasing or decreasing responses to a given odor across concentrations, its concentration response curve (described above) was fitted with a line and its slope was compared to the distribution of slopes obtained by shuffling the concentration labels. An odor response curve was called monotonically increasing (decreasing) if the slope was larger (smaller) than the 95% (5%) percentile of the slopes of the shuffled distributions.

The Odor Response Spectrum (ORS) for a given ROI was described as the vector of length equally to number of odors used, containing the average responses across trials to each odor. Non-significant odors responses were set to 0. Similarity between the ORS of two ROIs, ORS_i and ORS_j, was defined as the un-centered correlation coefficient (equivalent to cosine of the angle) between the two vectors:

$$\text{similarity} = \frac{ORS_i \cdot ORS_j}{\sqrt{(ORS_i \cdot ORS_i)(ORS_j \cdot ORS_j)}}$$

Similarly, we defined the population response (Cell Response Spectrum [CRS]) to an odor for a given field of view (FOV) as the vector of responses of all ROIs in the FOV responsive to that odor. ROIs with non-significant responses were set to zero. Odor similarity between two population responses was also defined as the un-centered correlation coefficient between the population response vectors.

Distance from diagonal unity line before versus after muscimol or saline injection and a change index (CI) were calculated only for cells that showed a significant response before or after injection. Distance from diagonal unity line was defined as shortest distance (normal) to the identity diagonal line in the scatter plot of odor responses before and after injection. Absolute value of change index (CI_{abs}) was defined as:

$$CI_{abs} = \frac{|Response\ post\ injection - Response\ before\ injection|}{|Response\ post\ injection| + |Response\ before\ injection|}$$

Sign of distance from diagonal line and CI was positive if:

$$|Response\ post\ injection| \geq |Response\ before\ injection|$$

and negative if:

$$|Response\ post\ injection| < |Response\ before\ injection|.$$

Most mitral and tufted cell GCaMP3 odor responses (> 90%) were positive. Hence, the use of absolute values did not affect our conclusions.

SUPPLEMENTAL INFORMATION

Supplemental Information includes Supplemental Experimental Procedures, eight figures, one table, and five movies and can be found with this article online at <http://dx.doi.org/10.1016/j.neuron.2015.05.023>.

AUTHOR CONTRIBUTIONS

G.H.O., H.C., and D.F.A. conceptualized the study and contributed to the practical design of experiments and analysis. G.H.O. and H.C. performed OB imaging and APC electrical stimulation and silencing experiments. M.B.D. performed viral injections and immunohistochemistry. G.H.O., H.C., and D.F.A. wrote the manuscript.

ACKNOWLEDGMENTS

We would like to thank P. Gupta for valuable input on manuscript preparation and A. Dăbăcan, A. Banerjee, and members of the D.F.A. laboratory for comments on the manuscript. This study was supported by a Pew Scholarship, Whitehall Fellowship and CSHL startup funds. In memoriam Mihai Pătrașcu.

Received: September 2, 2014

Revised: February 21, 2015

Accepted: May 7, 2015

Published: June 4, 2015

REFERENCES

- Akerboom, J., Chen, T.-W., Wardill, T.J., Tian, L., Marvin, J.S., Mutlu, S., Calderón, N.C., Esposti, F., Borghuis, B.G., Sun, X.R., et al. (2012). Optimization of a GCaMP calcium indicator for neural activity imaging. *J. Neurosci.* *32*, 13819–13840.
- Babadi, B., and Sompolinsky, H. (2014). Sparseness and expansion in sensory representations. *Neuron* *83*, 1213–1226.
- Balu, R., Pressler, R.T., and Strowbridge, B.W. (2007). Multiple modes of synaptic excitation of olfactory bulb granule cells. *J. Neurosci.* *27*, 5621–5632.
- Barak, O., Rigotti, M., and Fusi, S. (2013). The sparseness of mixed selectivity neurons controls the generalization-discrimination trade-off. *J. Neurosci.* *33*, 3844–3856.
- Boyd, A.M., Sturgill, J.F., Poo, C., and Isaacson, J.S. (2012). Cortical feedback control of olfactory bulb circuits. *Neuron* *76*, 1161–1174.
- Burton, S.D., and Urban, N.N. (2014). Greater excitability and firing irregularity of tufted cells underlies distinct afferent-evoked activity of olfactory bulb mitral and tufted cells. *J. Physiol.* *592*, 2097–2118.
- Caron, S.J.C., Ruta, V., Abbott, L.F., and Axel, R. (2013). Random convergence of olfactory inputs in the *Drosophila* mushroom body. *Nature* *497*, 113–117.
- Devore, S., and Linstner, C. (2012). Noradrenergic and cholinergic modulation of olfactory bulb sensory processing. *Front. Behav. Neurosci.* *6*, 52.
- Dhawale, A.K., Hagiwara, A., Bhalla, U.S., Murthy, V.N., and Albeanu, D.F. (2010). Non-redundant odor coding by sister mitral cells revealed by light addressable glomeruli in the mouse. *Nat. Neurosci.* *13*, 1404–1412.
- Fenno, L.E., Mattis, J., Ramakrishnan, C., Hyun, M., Lee, S.Y., He, M., Tucciarone, J., Selimbeyoglu, A., Berndt, A., Grosenick, L., et al. (2014). Targeting cells with single vectors using multiple-feature Boolean logic. *Nat. Methods* *11*, 763–772.
- Franks, K.M., Russo, M.J., Sosulski, D.L., Mulligan, A.A., Siegelbaum, S.A., and Axel, R. (2011). Recurrent circuitry dynamically shapes the activation of piriform cortex. *Neuron* *72*, 49–56.
- Fukunaga, I., Berning, M., Kollo, M., Schmaltz, A., and Schaefer, A.T. (2012). Two distinct channels of olfactory bulb output. *Neuron* *75*, 320–329.
- Ghosh, S., Larson, S.D., Hefzi, H., Marnoy, Z., Cutforth, T., Dokka, K., and Baldwin, K.K. (2011). Sensory maps in the olfactory cortex defined by long-range viral tracing of single neurons. *Nature* *472*, 217–220.
- Gilbert, C.D., and Li, W. (2013). Top-down influences on visual processing. *Nat. Rev. Neurosci.* *14*, 350–363.
- Glickfeld, L.L., Andermann, M.L., Bonin, V., and Reid, R.C. (2013). Cortico-cortical projections in mouse visual cortex are functionally target specific. *Nat. Neurosci.* *16*, 219–226.
- Gottfried, J.A. (2010). Central mechanisms of odour object perception. *Nat. Rev. Neurosci.* *11*, 628–641.
- Gray, C.M., and Skinner, J.E. (1988). Centrifugal regulation of neuronal activity in the olfactory bulb of the waking rabbit as revealed by reversible cryogenic blockade. *Exp. Brain Res.* *69*, 378–386.
- Guizar-Sicairos, M., Thurman, S.T., and Fienup, J.R. (2008). Efficient subpixel image registration algorithms. *Opt. Lett.* *33*, 156–158.
- Haberly, L.B. (2001). Parallel-distributed processing in olfactory cortex: new insights from morphological and physiological analysis of neuronal circuitry. *Chem. Senses* *26*, 551–576.
- Haberly, L.B., and Bower, J.M. (1989). Olfactory cortex: model circuit for study of associative memory? *Trends Neurosci.* *12*, 258–264.
- Haddad, R., Lanjuin, A., Madisen, L., Zeng, H., Murthy, V.N., and Uchida, N. (2013). Olfactory cortical neurons read out a relative time code in the olfactory bulb. *Nat. Neurosci.* *16*, 949–957.
- Harris, K.D., and Mrsic-Flogel, T.D. (2013). Cortical connectivity and sensory coding. *Nature* *503*, 51–58.
- Igarashi, K.M., Ieki, N., An, M., Yamaguchi, Y., Nagayama, S., Kobayakawa, K., Kobayakawa, R., Tanifuji, M., Sakano, H., Chen, W.R., and Mori, K. (2012). Parallel mitral and tufted cell pathways route distinct odor information to different targets in the olfactory cortex. *J. Neurosci.* *32*, 7970–7985.
- Jarosiewicz, B., Schummers, J., Malik, W.Q., Brown, E.N., and Sur, M. (2012). Functional biases in visual cortex neurons with identified projections to higher cortical targets. *Curr. Biol.* *22*, 269–277.
- Johnson, B.A., and Leon, M. (2007). Chemotopic odorant coding in a mammalian olfactory system. *J. Comp. Neurol.* *503*, 1–34.
- Kaplan, B.A., and Lansner, A. (2014). A spiking neural network model of self-organized pattern recognition in the early mammalian olfactory system. *Front. Neural Circuits* *8*, 5.
- Laurent, G. (2002). Olfactory network dynamics and the coding of multidimensional signals. *Nat. Rev. Neurosci.* *3*, 884–895.
- Linstner, C., and Hasselmo, M.E. (2001). Neuromodulation and the functional dynamics of piriform cortex. *Chem. Senses* *26*, 585–594.
- Ma, L., Qiu, Q., Gradwohl, S., Scott, A., Yu, E.Q., Alexander, R., Wiegand, W., and Yu, C.R. (2012). Distributed representation of chemical features and tonotopic organization of glomeruli in the mouse olfactory bulb. *Proc. Natl. Acad. Sci. USA* *109*, 5481–5486.
- Manabe, H., and Mori, K. (2013). Sniff rhythm-paced fast and slow gamma-oscillations in the olfactory bulb: relation to tufted and mitral cells and behavioral states. *J. Neurophysiol.* *110*, 1593–1599.
- Margrie, T.W., Sakmann, B., and Urban, N.N. (2001). Action potential propagation in mitral cell lateral dendrites is decremental and controls recurrent and lateral inhibition in the mammalian olfactory bulb. *Proc. Natl. Acad. Sci. USA* *98*, 319–324.
- Markopoulos, F., Rokni, D., Gire, D.H., and Murthy, V.N. (2012). Functional properties of cortical feedback projections to the olfactory bulb. *Neuron* *76*, 1175–1188.
- Matsutani, S. (2010). Trajectory and terminal distribution of single centrifugal axons from olfactory cortical areas in the rat olfactory bulb. *Neuroscience* *169*, 436–448.
- McCollum, J., Larson, J., Otto, T., Schottler, F., Granger, R., and Lynch, G. (1991). Short-latency single unit processing in olfactory cortex. *J. Cogn. Neurosci.* *3*, 293–299.

- Miura, K., Mainen, Z.F., and Uchida, N. (2012). Odor representations in olfactory cortex: distributed rate coding and decorrelated population activity. *Neuron* 74, 1087–1098.
- Miyamichi, K., Amat, F., Moussavi, F., Wang, C., Wickersham, I., Wall, N.R., Taniguchi, H., Tasic, B., Huang, Z.J., He, Z., et al. (2011). Cortical representations of olfactory input by trans-synaptic tracing. *Nature* 472, 191–196.
- Nagayama, S., Takahashi, Y.K., Yoshihara, Y., and Mori, K. (2004). Mitral and tufted cells differ in the decoding manner of odor maps in the rat olfactory bulb. *J. Neurophysiol.* 91, 2532–2540.
- Nagayama, S., Enerva, A., Fletcher, M.L., Masurkar, A.V., Igarashi, K.M., Mori, K., and Chen, W.R. (2010). Differential axonal projection of mitral and tufted cells in the mouse main olfactory system. *Front Neural Circuits* 4, 120.
- Nakashima, M., Mori, K., and Takagi, S.F. (1978). Centrifugal influence on olfactory bulb activity in the rabbit. *Brain Res.* 154, 301–306.
- Nunez-Parra, A., Maurer, R.K., Krahe, K., Smith, R.S., and Araneda, R.C. (2013). Disruption of centrifugal inhibition to olfactory bulb granule cells impairs olfactory discrimination. *Proc. Natl. Acad. Sci. USA* 110, 14777–14782.
- Oswald, A.-M., and Urban, N.N. (2012). There and back again: the corticobulbar loop. *Neuron* 76, 1045–1047.
- Otazu, G.H., and Leibold, C. (2011). A corticothalamic circuit model for sound identification in complex scenes. *PLoS ONE* 6, e24270.
- Peteanu, L., Gutnisky, D.A., Huber, D., Xu, N.L., O'Connor, D.H., Tian, L., Looger, L., and Svoboda, K. (2012). Activity in motor-sensory projections reveals distributed coding in somatosensation. *Nature* 489, 299–303.
- Petzold, G.C., Hagiwara, A., and Murthy, V.N. (2009). Serotonergic modulation of odor input to the mammalian olfactory bulb. *Nat. Neurosci.* 12, 784–791.
- Poo, C., and Isaacson, J.S. (2009). Odor representations in olfactory cortex: “sparse” coding, global inhibition, and oscillations. *Neuron* 62, 850–861.
- Ranade, S.P., and Mainen, Z.F. (2009). Transient firing of dorsal raphe neurons encodes diverse and specific sensory, motor, and reward events. *J. Neurophysiol.* 102, 3026–3037.
- Rao, R.P., and Ballard, D.H. (1999). Predictive coding in the visual cortex: a functional interpretation of some extra-classical receptive-field effects. *Nat. Neurosci.* 2, 79–87.
- Rothermel, M., and Wachowiak, M. (2014). Functional imaging of cortical feedback projections to the olfactory bulb. *Front. Neural Circuits* 8, 73.
- Sallaz, M., and Jourdan, F. (1993). C-fos expression and 2-deoxyglucose uptake in the olfactory bulb of odour-stimulated awake rats. *Neuroreport* 4, 55–58.
- Sato, T.R., and Svoboda, K. (2010). The functional properties of barrel cortex neurons projecting to the primary motor cortex. *J. Neurosci.* 30, 4256–4260.
- Shepherd, G.M. (1972). Synaptic organization of the mammalian olfactory bulb. *Physiol. Rev.* 52, 864–917.
- Shipley, M.T., and Adamek, G.D. (1984). The connections of the mouse olfactory bulb: a study using orthograde and retrograde transport of wheat germ agglutinin conjugated to horseradish peroxidase. *Brain Res. Bull.* 12, 669–688.
- Sosulski, D.L., Bloom, M.L., Cutforth, T., Axel, R., and Datta, S.R. (2011). Distinct representations of olfactory information in different cortical centres. *Nature* 472, 213–216.
- Soucy, E.R., Albeanu, D.F., Fantana, A.L., Murthy, V.N., and Meister, M. (2009). Precision and diversity in an odor map on the olfactory bulb. *Nat. Neurosci.* 12, 210–220.
- Stettler, D.D., and Axel, R. (2009). Representations of odor in the piriform cortex. *Neuron* 63, 854–864.
- Suzuki, N., and Bekkers, J.M. (2011). Two layers of synaptic processing by principal neurons in piriform cortex. *J. Neurosci.* 31, 2156–2166.
- Taniguchi, H., He, M., Wu, P., Kim, S., Paik, R., Sugino, K., Kvitsiani, D., Fu, Y., Lu, J., Lin, Y., et al. (2011). A resource of Cre driver lines for genetic targeting of GABAergic neurons in cerebral cortex. *Neuron* 71, 995–1013.
- Tian, L., Hires, S.A., Mao, T., Huber, D., Chiappe, M.E., Chalasani, S.H., Petreanu, L., Akerboom, J., McKinney, S.A., Schreiter, E.R., et al. (2009). Imaging neural activity in worms, flies and mice with improved GCaMP calcium indicators. *Nat. Methods* 6, 875–881.
- Tobin, V.A., Hashimoto, H., Wacker, D.W., Takayanagi, Y., Langnaese, K., Caquineau, C., Noack, J., Landgraf, R., Onaka, T., Leng, G., et al. (2010). An intrinsic vasopressin system in the olfactory bulb is involved in social recognition. *Nature* 464, 413–417.
- Uchida, N., Takahashi, Y.K., Tanifuji, M., and Mori, K. (2000). Odor maps in the mammalian olfactory bulb: domain organization and odorant structural features. *Nat. Neurosci.* 3, 1035–1043.
- Urban, N.N., and Sakmann, B. (2002). Reciprocal intraglomerular excitation and intra- and interglomerular lateral inhibition between mouse olfactory bulb mitral cells. *J. Physiol.* 542, 355–367.
- Vélez-Fort, M., Rousseau, C.V., Niedworok, C.J., Wickersham, I.R., Rancz, E.A., Brown, A.P.Y., Strom, M., and Margrie, T.W. (2014). The stimulus selectivity and connectivity of layer six principal cells reveals cortical microcircuits underlying visual processing. *Neuron* 83, 1431–1443.
- Vickers, N.J. (2000). Mechanisms of animal navigation in odor plumes. *Biol. Bull.* 198, 203–212.
- Vinje, W.E., and Gallant, J.L. (2000). Sparse coding and decorrelation in primary visual cortex during natural vision. *Science* 287, 1273–1276.
- Wachowiak, M., Wesson, D.W., Pirez, N., Verhagen, J.V., and Carey, R.M. (2009). Low-level mechanisms for processing odor information in the behaving animal. *Ann. N Y Acad. Sci.* 1170, 286–292.
- Wiechert, M.T., Judkewitz, B., Riecke, H., and Friedrich, R.W. (2010). Mechanisms of pattern decorrelation by recurrent neuronal circuits. *Nat. Neurosci.* 13, 1003–1010.
- Willhite, D.C., Nguyen, K.T., Masurkar, A.V., Greer, C.A., Shepherd, G.M., and Chen, W.R. (2006). Viral tracing identifies distributed columnar organization in the olfactory bulb. *Proc. Natl. Acad. Sci. USA* 103, 12592–12597.
- Wilson, R.I., and Mainen, Z.F. (2006). Early events in olfactory processing. *Annu. Rev. Neurosci.* 29, 163–201.
- Wilson, D.A., and Sullivan, R.M. (2011). Cortical processing of odor objects. *Neuron* 72, 506–519.
- Wilson, D.A., Fletcher, M.L., and Sullivan, R.M. (2004). Acetylcholine and olfactory perceptual learning. *Learn. Mem.* 11, 28–34.
- Zariwala, H.A., Borghuis, B.G., Hoogland, T.M., Madisen, L., Tian, L., De Zeeuw, C.I., Zeng, H., Looger, L.L., Svoboda, K., and Chen, T.-W. (2012). A Cre-dependent GCaMP3 reporter mouse for neuronal imaging in vivo. *J. Neurosci.* 32, 3131–3141.
- Zhan, C., and Luo, M. (2010). Diverse patterns of odor representation by neurons in the anterior piriform cortex of awake mice. *J. Neurosci.* 30, 16662–16672.